Microchimica Acta (2018) 185: 44
https://doi.org/10.1007/s00604-017-2603-7

ORIGINAL PAPER

Detection of glutathione based on MnO_2 nanosheet-gated mesoporous silica nanoparticles and target induced release of glucose measured with a portable glucose meter

Qingqing Tan[1] · Ruirui Zhang[2] · Rongmei Kong[1] · Weisu Kong[1] · Wenzhi Zhao[1] · Fengli Qu[1]

Received: 22 September 2017 / Accepted: 1 December 2017 / Published online: 8 December 2017

Abstract
The authors describe a novel method for the determination of glutathione (GSH). Detection is based on target induced release of glucose from MnO_2 nanosheet-gated aminated mesoporous silica nanoparticles (MSNs). In detail, glucose is loaded into the pores of MSNs. Negatively charged MnO_2 nanosheets are assembled on the MSNs through electrostatic interactions. The nanosheets are reduced by GSH, and this results in the release of glucose which is quantified by using a commercial electrochemical glucose meter. GSH can be quantified by this method in the 100 nM to 10 μM concentration range, with a 34 nM limit of detection.

Keywords MnO_2 nanosheets · Mesoporous silica · Personal glucose meter · Glutathione · Portable detection · Target induced release

Introduction

Glutathione (GSH),the dominant nonprotein thiol in mammalian and eukaryotic cells, is synthesized endogenously from the precursor amino acids L-cysteine, L-glutamic acid, and glycine [1]. It participates in several vital biological functions, including protein and DNA synthesis, amino acid transport, enzyme activity, and maintenance of intracellular redox homeostasis, metabolism and detoxification [2]. Levels of GSH are associated with kinds of human diseases, such as cancer, HIV, AIDS, aging, and Alzheimer's disease [3–5]. Due to the biological and clinical significance, it is of sustained interest in accurate and selective quantification of GSH. Numbers of methods and strategies so far have focused on determination of GSH, e.g., high-performance liquid chromatography (HPLC) [6], electrochemistry [7], chemiluminescence [8], surface-enhanced Raman scattering (SERS) [9], mass spectrometry [10], and fluorescence spectroscopy [11–15]. These methods, however, not only require expensive instruments and sophisticated operations but also involve complicated sample pretreatment, which limits their applications in clinical diagnostics and treatment.

Point-of-care (POC) testing allows rapid, on-site, and affordable detection of biomarker at home, which brings considerable convenience to the patient. The personal glucose meter (PGM) is currently one of the most widely used diagnostic devices in POC testing because of its portable size, time-saving, low cost and reliable quantitative results [16]. Up to now, various PGM-based methods have been fabricated for quantitative detection of a wide range of non-glucose targets based on target-responsive controlled release of glucose from gated-mesoporous silica nanoparticles (MSNs) [17–22]. For example, Tang et al. constructed an immunoassay for quantitative detection of aflatoxins based on target-induced

Qingqing Tan and Ruirui Zhang contributed equally to this work.

Electronic supplementary material The online version of this article (https://doi.org/10.1007/s00604-017-2603-7) contains supplementary material, which is available to authorized users.

✉ Fengli Qu
fengliquhn@hotmail.com

[1] College of Chemistry and Chemical Engineering, Qufu Normal University, Qufu, Shandong 273165, People's Republic of China

[2] Beijing Key Laboratory of Ionic Liquids Clean Process, Key Laboratory of Green Process and Engineering, Institute of Process Engineering, Chinese Academy of Sciences, Beijing 100190, People's Republic of China

release of glucose from the Au nanoparticles-gated MSNs by coupling a competitive-type displacement reaction mode with PGM [23]. Lu et al. established an efficient approach to quantitatively monitor telomerase activity using DNA-capped MSNs by coupling with a PGM based on target-responsive release strategy [24]. Among these methods, MSNs exhibit exceptional biocompatibility, high surface area, large pore volume, and ease of functionalization, which make it possible to load large numbers of glucose by different gates and diverse design strategies.

Ultrathin MnO_2 nanosheets, one type of redox-active 2D nanomaterial, are composed of three atomic layers includes two O layers and one Mn layer. Each Mn is coordinated to six O atoms to form an edge-sharing MnO_6 octahedron [25]. As a result of the presence of Mn-vacancies, single-layer MnO_2 nanosheets were negatively charged [26]. At the same time, MnO_2 nanosheets with strong oxidation ability can be reduced into Mn^{2+} by GSH, dithiothreitol and ascorbic acid [27–29]. These together led to the successful development of diverse assay platforms for GSH detection [30, 31]. Therefore, MnO_2 nanosheets provide the possibility for fabricating portable, rapid and cost-effective PGM-based detection device for GSH detection.

We report a novel approach for rapid and selective detection of GSH using a PGM based, target-responsive release of glucose from MnO_2 nanosheet-gated MSNs. Glucose was successfully loaded in the pores of the aminated MSNs, which were then coated by negatively charged MnO_2 nanosheets via electrostatic interaction. The MnO_2 nanosheets served as "gates" to prevent the release of the glucose. In the presence of GSH, MnO_2 nanosheets can be reduced into Mn^{2+}, leading to open the gates and induce the release of glucose from the pore. The released glucose can be monitored using an external PGM. By evaluation of the PGM signal, the concentration of GSH in the sample can be calculated.

Experimental section

Reagents and materials

Glutathione (GSH) (reduced form) was purchased from Aladdin Chemical (Shanghai, China, www.aladdin-e.com). Tetramethylammonium hydroxide, manganese chloride tetrahydrate ($MnCl_2$ $4H_2O$),(3-aminopropyl) triethoxysilane (APTES), glucose, glutamic acid (Glu), glycine (Gly), aspartic acid (Asp), tyrosine (Tyr), lysine (Lys), and ascorbic acid (AA) were purchased from Sigma-Aldrich (USA, www.sigma-aldrich.com). Tetraethyl orthosilicate (TEOS), hexadecyl trimethylammonium bromide (CTAB), aqueous ammonia solution ($NH_3 \cdot H_2O$, 28%), methanol, sodium hydroxide (NaOH), sodium chloride (NaCl), potassium chloride (KCl), calcium chloride ($CaCl_2$) and manganese chloride ($MnCl_2$) were bought from Sinopharm Chemical Reagent Co., Ltd. (Shang hai, China, www.sino-reagent.com). Other reagents were of analytical grade and used without further purification. All solutions were prepared with Milli-Q water (resistivity > 18 MΩ cm) from a Millipore system.

Apparatus

Transmission electron microscopy (TEM) images were carried out on a JEM-2100 PLUS microscope (Japan, https://www.jeol.co.jp/en, Japan) at an acceleration voltage of 200 kV. Ultraviolet-visible (UV-vis) absorption spectra were measured using a Varian Cary-300 bio UV/vis spectrophotometer (USA, https://www.varian.com). The zeta potential was determined by Apparatus Mk II microelectrophoresis (England, http://www.rankbrothers.co.uk). All glucose levels were recorded using a PGM (China, http://www.sinocare.com).

Detection of GSH

The glucose-loading MSNs capped with MnO_2 nanosheets (MSNs-G@MnO_2) were prepared according to the literatures [24, 32]. 50 μL of GSH at various concentrations were added into 100 μL of the glucose-loading MSNs capped with MnO_2 nanosheets (MSNs-G@MnO_2). The samples were shaken occasionally during the reaction at room temperature. During this process, GSH reduces MnO_2 to Mn^{2+}, which results in the destruction of the MnO_2 nanosheets and causes the release of glucose. After incubation for 10 min, the concentration of released glucose was determined by a commercially available PGM.

Results and discussion

Choice of materials

MSNs have high pore volume, large surface area, controlled particles size, and excellent biocompatibility. They are promising candidates for loading a wide range of substances [24]. MnO_2 nanosheets,two-dimensional layered materials, with high specific surface area and super light absorption capacity, which has attracted significant attention in developing covering-type and "turn-off-on" fluorescence sensing platforms [32]. In addition, MnO_2 nanosheets can be reduced to Mn^{2+} by some reducing substances. Taking into account its abilities of covering and oxidation, we selected MnO_2 nanosheets to construct GSH detection platform.

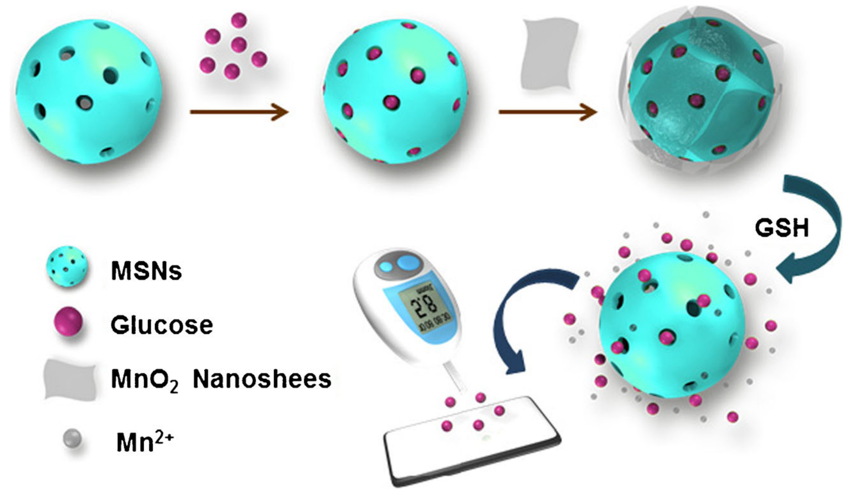

Scheme 1 Schematic illustration for quantitative detection of glutathione using an external PGM

Detection mechanism

The detection of GSH is based on the target-responsive release of glucose from MnO_2-nanosheet-gated mesoporous silica nanoparticles (MSNs-G@MnO_2, Scheme 1). Noticeable amounts of glucose are firstly loaded into the pores of MSNs due to the strong preferential interaction between glucose and silica walls [33]. Then, the gates of positively charged aminated MSNs are sealed by negatively charged MnO_2 nanosheets due to the electrostatic interaction. Upon the introduction of GSH, the MSN-G@MnO_2 is gradually falling apart since GSH reduces MnO_2 to form Mn^{2+} ions. This leads to the decomposition of the MnO_2 nanosheets. As a result, the "gate" is destroyed and allows the pore-trapped glucose to diffuse out of MSNs for PGM detection. In this case, the acquired PGM signal is directly proportional to GSH concentration.

Characterization of MnO_2-nanosheet-gated MSNs

Amino groups were introduced on the outlet of MSNs using established methods [24]. As shown from column "a" in Fig. 1a, the zeta potential of the aminated MSNs was 7.27 mV, indicating that APTES was successfully conjugated onto the MSNs to display positively charged nature. Since the MnO_2 nanosheets exhibited a negative zeta potential (−11.9 mV), when aminated MSNs were coated by MnO_2 nanosheets, the zeta potential became more negative (−17.6 mV) (Fig. 1a). This indicates that MnO_2 nanosheets can be assembled onto aminated MSN by electrostatic interaction. Figure 1b shows typical TEM image of the aminated

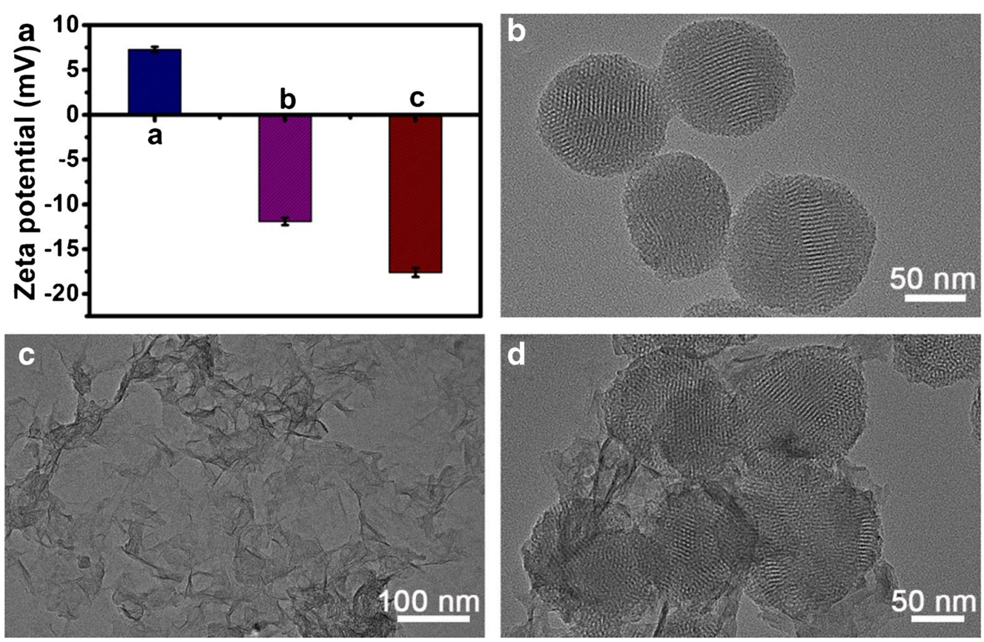

Fig. 1 (**a**) Zeta potentials of *a* the aminated MSNs, *b* MnO_2 nanosheets and *c* MnO_2 nanosheets-coated MSNs. TEM images of (**b**) the aminated MSNs, (**c**) MnO_2 nanosheets and (**d**) MnO_2 nansheets-MSN nanoparticles

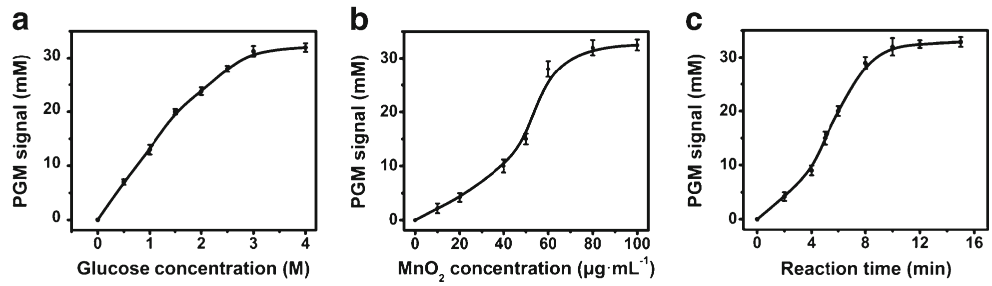

Fig. 2 Dependence of the PGM signal on (**a**) glucose concentration (**b**) MnO_2 nanosheets concentration and (**c**) release time of glucose ($C_{[GSH]}$ = 100 μM). The error bars were derived from the standard deviation of three measurements. Error bar = SD (n = 3)

MSNs with uniform, nearly spherical morphology and narrow size distribution. The aminated MSNs possess well-ordered nanopores, which provided sufficient space for glucose loading. Ultrathin MnO_2 nanosheets were prepared via a one-step approach [32]. As shown in Fig. 1c, MnO_2 nanosheets displayed a large 2D and ultrathin plane with occasional folds and wrinkles. The formation of MnO_2 nanosheets-MSNs was also confirmed by TEM (Fig. 1d), which indicated that MnO_2 nanosheets can be assembled onto the surface of aminated MSNs and the MnO_2 nansheets-MSNs can serve as an ideal nanocontainer for encapsulating glucose.

Optimization of method

Before optimizing experimental conditions, we studied the stability of the MSNs-G@MnO_2 system (Figure S1). After that, the following parameters were optimized: (a) concentration of glucose (Fig. 2a); (b) concentration of MnO_2 nanosheets (Fig. 2b); (c) releasing time for glucose (Fig. 2c). Respective data and Figures are given in ESM. We found the following experimental conditions to give best results: (a) Concentration of glucose: 3 M; (b) Concentration of MnO_2 nanosheets: 80 μg·mL^{-1}; (c) Release time for glucose: 6 min.

Analytical performance of PGM-based nanoprobe toward GSH detection

Under the optimal conditions, the PGM-based nanoprobe was employed for quantifying GSH with various concentrations based on target-responsive controlled release of glucose from MSNs-G@MnO_2. The detection was carried out using an external PGM after GSH reacted with MSNs-G@MnO_2 for 6 min at room temperature. As shown in Fig. 3a, the PGM signal increased with the increasing GSH concentration. A linear dependence between PGM signal (mM) and GSH level (μM) was achieved in the range from 100 nM to 10 μM. The linear regression equation was Y (mM) = 1.0497 + 0.9184 × $C_{[GSH]}$ (μM), R^2 = 0.9943. The limit of detection (LOD) was 34 nM, as calculated in terms of the rule of 3× standard deviation over the blank signal. Compared with other methods determination of GSH reported previously [7, 11, 15, 25, 30], our method gave lower or comparable detection limit (Table 1).

To investigate the selectivity of the MSNs-G@MnO_2 nanoprobe for GSH, the PGM signals were recorded in the presence of potential interferences, including a wide range of electrolytes and biological species (GSH at a concentration of 10 μM and all other compounds at concentrations of 10 mM).

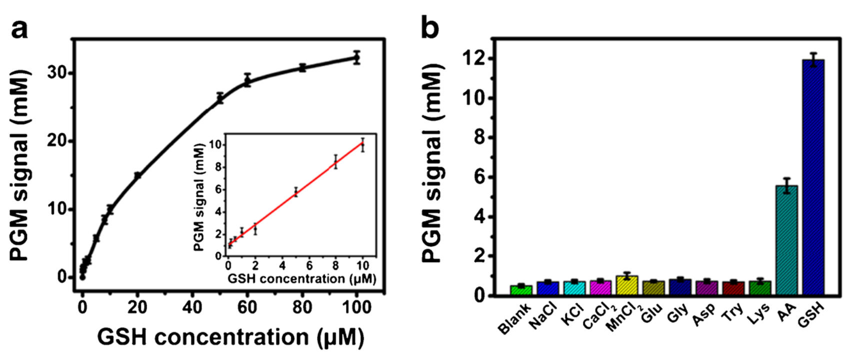

Fig. 3 (**a**) Relationship between PGM signal and the GSH concentration. Inset shows a linear standard plot between PGM signal and the GSH concentration. (**b**) Selectivity of MSNs-G@MnO_2 nanoparticles for GSH over other potential interferences. The error bars were derived from the standard deviation of three measurements. Error bar = SD (n = 3)

Table 1 Comparison of this method with the newly reported approaches for GSH determination

Materials	Methods	Linear range (μM)	Linear range (nM)	Ref.
Carbon dots–Ni(IV)	Chemiluminescence	0.31–31	200	[7]
Carbon dots	Fluorescence	0–175	110	[15]
UCNPs- MnO_2[a]	Fluorescence	0–10,000	900	[30]
NMM[b]	Fluorescence	0.01-0.6	3.5	[11]
iridium(III)complex-MnO_2[c]	Fluorescence	1-200	130	[25]
MSNs-G@MnO_2[d]	PGM-based	0.1–10	34	This work

[a] Upconversion nanoparticles modified with MnO_2-nanosheets

[b] N-methylmesoporphyrin IX

[c] Iridium(III) complex $[Ir(Cl\text{-}phq)_2(Cl\text{-}phen)]^+$ assisted with MnO_2-nanosheets

[d] Glucose-loading MSNs capped with MnO_2 nanosheets

Among them, only reducing biomolecules (AA and GSH) caused comparatively high PGM signals, while amino acids and electrolytes did not induce an obvious increase in the PGM signal (Fig. 3b). Although AA can also cause a response to this system, its concentrations (μM levels) are relatively lower than that of GSH (mM levels) in biological systems [34, 35]**.** In addition, other thiols, such as cysteine, homocysteine have little effect on this system [14, 25, 27, 31]. Moreover, owing to the ideal sensitivity of our strategy, the serum sample needed to be diluted before the measurement. Under such conditions, the concentration of AA would be at nM level, and would not cause interference to the assay. Thus, the specificity of MSNs-G@MnO_2 nanoprobe was acceptable, which makes it a promising method for the detection of GSH in biological samples.

Application analysis in serum samples

In order to estimate the potential applicability in complex biological samples, MSNs-G@MnO_2 was applied to detect GSH in human blood samples. The accuracy of the sample analysis was measured by calculating the recovery of spiking a known amount of standard GSH in three 100-fold diluted human serum samples. The total analytical results are summarized in Table 1. 2 μM and 4 μM of GSH were added into each serum samples, respectively. The recovery of GSH is ranged from 97.5% to 102.5%, and the RSD is ranged from 1.9% to 3.5%**.** These results indicated that the MSNs-G@MnO_2 nanoparticles had the advantages of being low-cost, rapid, and portable, which can be available for GSH detection in clinical applications (Table 2).

Conclusions

We have successfully designed a portable, sensitive sensor for quantitative detection of GSH using a PGM based on the target-induced release of glucose from MnO_2-nanosheet-gated MSNs. Interestingly, this detection method is fast and convenient. In addition, this method exhibits a good linear response to the concentration range from 100 nM to 10 μM with a detection limit of 34 nM. More importantly, compared with the standard instrumental sensing methods, this PGM-based assay system is low-cost, rapid, portable and user-friendly. Thus, the strategy can be used for quantitative detection of a wide range of non-glucose targets.

Table 2 Recoveries results of the determination of GSH in diluted serum samples

Sample	Determined GSH (μM)	Spiked (μM)	Measured (μM)	Recovery[a] (%)	RSD (n = 3)
1	4.10	2	6.05	97.5	2.1
		4	8.09	102.3	2.8
2	4.25	2	6.28	101.5	2.9
		4	8.20	98.8	3.5
3	4.30	2	6.35	102.5	1.9
		4	8.26	99.0	2.6

[a] Mean value of three independent measurements

Acknowledgements The authors are grateful for the support of the National Natural Science Foundation of China (21775089, 21375076, 21705151), the Project of Shandong Province Science and Technology Program (2015GSF121031), Outstanding Youth Foundation of Shandong Province (ZR2017JL010), and the Project of Beijing National Science Foundation (2174085).

Compliance with ethical standards The author(s) declare that they have no competing interests.

References

1. SC L (1999) Regulation of hepatic glutathione synthesis: current concepts and controversies. FASEB J 13:1169–1183
2. Lu SC (2009) Regulation of glutathione synthesis. Mol Asp Med 30:42–59
3. Estrela JM, Ortega A, Obrador E (2006) Glutathione in cancer biology and therapy. Crit Rev Clin Lab Sci 43:143–181
4. Herzenberg LA, De Rosa SC, Dubs JG, Roederer M, Anderson MT, Ela SW, Deresinski SC, Herzenberg LA (1997) Glutathione deficiency is associated with impaired survival in HIV disease. Proc Natl Acad Sci 94:1967–1972
5. Townsend DM, Tew KD, Tapiero H (2003) The importance of glutathione in human disease. Biomed Pharmacother 57:145–155
6. Reed D, Babson J, Beatty P, Brodie A, Ellis W, Potter D (1980) High-performance liquid chromatography analysis of nanomole levels of glutathione, glutathione disulfide, and related thiols and disulfides. Anal Biochem 106:55–62
7. Çubukçu M, Ertaş FN, Anık Ü (2013) Centri-voltammetric determination of glutathione. Microchim Acta 180:93–100
8. Dong Y, Su M, Chen P, Sun H (2015) Chemiluminescence of carbon dots induced by diperiodato-nicklate (IV) in alkaline solution and its application to a quenchometric flow-injection assays of paracetamol, L-cysteine and glutathione. Microchim Acta 182: 1071–1077
9. Saha A, Jana NR (2013) Detection of cellular glutathione and oxidized glutathione using magnetic-plasmonic nanocomposite-based "turn-off" surface enhanced Raman scattering. Anal Chem 85: 9221–9228
10. Zhu X, Kalyanaraman N, Subramanian R (2011) Enhanced screening of glutathione-trapped reactive metabolites by in-source collision-induced dissociation and extraction of product ion using UHPLC-high resolution mass spectrometry. Anal Chem 83:9516–9523
11. Ji D, Meng H, Ge J, Zhang L, Wang H, Bai D, Li J, Qu L, Li Z (2017) Ultrasensitive fluorometric glutathione assay based on a conformational switch of a G-quadruplex mediated by silver (I). Microchim Acta 184:3325–3332
12. Tang B, Xing Y, Li P, Zhang N, Yu F, Yang G (2007) A rhodamine-based fluorescent probe containing a Se-N bond for detecting thiols and its application in living cells. J Am Chem Soc 129:11666–11667
13. Wu D, Li G, Chen X, Qiu N, Shi X, Chen G, Sun Z, You J, Wu Y (2017) Fluorometric determination and imaging of glutathione based on a thiol-triggered inner filter effect on the fluorescence of carbon dots. Microchim Acta 184:1923–1931
14. Li N, Diao W, Han Y, Pan W, Zhang T, Tang B (2014) MnO_2-modified persistent luminescence nanoparticles for detection and imaging of glutathione in living cells and in vivo. Chem Eur J 20: 16488–16491
15. Yang R, Guo X, Jia L, Zhang Y (2017) A fluorescent "on-off-on" assay for selective recognition of Cu (II) and glutathione based on modified carbon nanodots, and its application to cellular imaging. Microchim Acta 184:1143–1150
16. Hou L, Zhu C, Wu X, Chen G, Tang D (2014) Bioresponsive controlled release from mesoporous silica nanocontainers with glucometer readout. Chem Commun 50:1441–1443
17. Zhang R, Li L, Feng J, Tong L, Wang Q, Tang B (2014) Versatile triggered release of multiple molecules from cyclodextrin-modified gold-gated mesoporous silica nanocontainers. ACS Appl Mater Interfaces 6:9932–9936
18. Yang M, Li H, Javadi A, Gong S (2010) Multifunctional mesoporous silica nanoparticles as labels for the preparation of ultrasensitive electrochemical immunosensors. Biomaterials 31:3281–3286
19. Pan W, Wang H, Yang L, Yu Z, Li N, Tang B (2016) Ratiometric fluorescence nanoprobes for subcellular pH imaging with a single-wavelength excitation in living cells. Anal Chem 88:6743–6748
20. Chen S, Zhang J, Gan N, Hu F, Li T, Cao Y, Pan D (2015) An on-site immunosensor for ractopamine based on a personal glucose meter and using magnetic β-cyclodextrin-coated nanoparticles for enrichment, and an invertase-labeled nanogold probe for signal amplification. Microchim Acta 182:815–822
21. Li N, Yu Z, Pan W, Han Y, Zhang T, Tang B (2013) A near-infrared light-triggered nanocarrier with reversible DNA valves for intracellular controlled release. Adv Funct Mater 23:2255–2262
22. Li Y, Li N, Pan W, Yu Z, Yang L, Tang B (2017) Hollow mesoporous silica nanoparticles with tunable structures for controlled drug delivery. ACS Appl Mater Interfaces 9:2123–2129
23. Tang D, Lin Y, Zhou Q, Lin Y, Li P, Niessner R, Knopp D (2014) Low-cost and highly sensitive immunosensing platform for aflatoxins using one-step competitive displacement reaction mode and portable glucometer-based detection. Anal Chem 86: 11451–11458
24. Wang Y, Lu M, Zhu J, Tian S (2014) Wrapping DNA-gated mesoporous silica nanoparticles for quantitative monitoring of telomerase activity with glucometer readout. J Mater Chem B 2: 5847–5853
25. Dong Z-Z, Lu L, Ko C-N, Yang C, Li S, Lee M-Y, Leung C-H, Ma D-L (2017) A MnO_2 nanosheet-assisted GSH detection platform using an iridium (iii) complex as a switch-on luminescent probe. Nano 9:4677–4682
26. Zhang X, Kong R, Tan Q, Qu F, Qu F (2017) A label-free fluorescence turn-on assay for glutathione detection by using MnO_2 nanosheets assisted aggregation-induced emission-silica nanospheres. Talanta 169:1–7
27. He D, Yang X, He X, Wang K, Yang X, He X, Zou Z (2015) A sensitive turn-on fluorescent probe for intracellular imaging of glutathione using single-layer MnO_2 nanosheet-quenched fluorescent carbon quantum dots. Chem Commun 51:14764–14767
28. Meng H, Jin Z, Lv Y, Yang C, Zhang X-B, Tan W, R-Q Y (2014) Activatable two-photon fluorescence nanoprobe for bioimaging of glutathione in living cells and tissues. Anal Chem 86:12321–12326
29. Qu F, Pei H, Kong R, Zhu S, Xia L (2017) Novel turn-on fluorescent detection of alkaline phosphatase based on green synthesized carbon dots and MnO_2 nanosheets. Talanta 165:136–142
30. Deng R, Xie X, Vendrell M, Chang Y-T, Liu X (2011) Intracellular glutathione detection using MnO_2-nanosheet-modified upconversion nanoparticles. J Am Chem Soc 133: 20168–20171

31. Kong X-J, Wu S, Chen T-T, R-Q Y, Chu X (2016) MnO_2-induced synthesis of fluorescent polydopamine nanoparticles for reduced glutathione sensing in human whole blood. Nano 8:15604–15610
32. Kai K, Yoshida Y, Kageyama H, Saito G, Ishigaki T, Furukawa Y, Kawamata J (2008) Room-temperature synthesis of manganese oxide monosheets. J Am Chem Soc 130:15938–15943
33. Ziemys A, Grattoni A, Fine D, Hussain F, Ferrari M (2010) Confinement effects on monosaccharide transport in nanochannels. J Phys Chem B 114:11117–11126
34. Kong W, Wu D, Li G, Chen X, Gong P, Sun Z, Chen G, Xia L, You J, Wu Y (2017) A facile carbon dots based fluorescent probe for ultrasensitive detection of ascorbic acid in biological fluids via non-oxidation reduction strategy. Talanta 165:677–684
35. Lu S, Wu D, Li G, Lv Z, Chen Z, Chen L, Chen G, Xia L, You J, Wu Y (2016) Carbon dots-based ratiometric nanosensor for highly sensitive and selective detection of mercury (II) ions and glutathione. RSC Adv 6:103169–103177